10. Kang, T. M., Markin, V. S. & Hilgemann, D. W. Ion fluxes in giant excised cardiac membrane patches detected and quantified with ion-selective microelectrodes. *J. Gen. Physiol.* **121,** 325–348 (2003).
11. DeFelice, L. J. & Galli, A. Fluctuation analysis of norepinephrine and serotonin transporter currents. *Methods Enzymol.* **296,** 578–593 (1998).
12. Mackenzie, B., Loo, D. D. & Wright, E. M. Relationships between Na^+/glucose cotransporter (SGLT1) currents and fluxes. *J. Membr. Biol.* **162,** 101–106 (1998).
13. Linck, B. *et al.* Functional comparison of the three isoforms of the Na^+/Ca^{2+} exchanger (NCX1, NCX2, NCX3). *Am. J. Physiol.* **274,** C415–C423 (1998).
14. Hilgemann, D. W., Nicoll, D. A. & Philipson, K. D. Charge movement during Na^+ translocation by native and cloned cardiac Na^+/Ca^{2+} exchanger. *Nature* **352,** 715–718 (1991).
15. Hilgemann, D. W. Unitary cardiac Na^+, Ca^{2+} exchange current magnitudes determined from channel-like noise and charge movements of ion transport. *Biophys. J.* **71,** 759–768 (1996).
16. Robinson, R. A. & Stokes, R. H. *Electrolyte solutions* (Butterworths, London, 2002).
17. Hilgemann, D. W. Regulation and deregulation of cardiac Na^+-Ca^{2+} exchange in giant excised sarcolemmal membrane patches. *Nature* **344,** 242–245 (1990).
18. Wang, E. *et al.* Transport properties of the calcium ionophore ETH-129. *Biophys. J.* **81,** 3275–3284 (2001).
19. Rakowski, R. F., Gadsby, D. C. & De Weer, P. Stoichiometry and voltage dependence of the sodium pump in voltage-clamped, internally dialyzed squid giant axon. *J. Gen. Physiol.* **93,** 903–941 (1989).
20. Reeves, J. P. & Sutko, J. L. Competitive interactions of sodium and calcium with the sodium-calcium exchange system of cardiac sarcolemmal vesicles. *J. Biol. Chem.* **258,** 3178–3182 (1983).
21. Matsuoka, S. & Hilgemann, D. W. Steady-state and dynamic properties of cardiac sodium-calcium exchange. Ion and voltage dependencies of the transport cycle. *J. Gen. Physiol.* **100,** 963–1001 (1992).
22. Kang, T. M., Steciuk, M. & Hilgemann, D. W. Sodium-calcium exchange stoichiometry: is the noose tightening? *Ann. NY Acad. Sci.* **976,** 142–151 (2002).
23. Niggli, E. & Lederer, W. J. Molecular operations of the sodium-calcium exchanger revealed by conformation currents. *Nature* **349,** 621–624 (1991).
24. Kappl, M. & Hartung, K. Rapid charge translocation by the cardiac Na^+-Ca^{2+} exchanger after a Ca^{2+} concentration jump. *Biophys. J.* **71,** 2473–2485 (1996).
25. Cervetto, L., Lagnado, L., Perry, R. J., Robinson, D. W. & McNaughton, P. A. Extrusion of calcium from rod outer segments is driven by both sodium and potassium gradients. *Nature* **337,** 740–743 (1989).
26. Hinata, M. *et al.* Stoichiometry of Na^+-Ca^{2+} exchange is 3:1 in guinea-pig ventricular myocytes. *J. Physiol. (Lond.)* **545,** 453–461 (2002).
27. Hilgemann, D. W., Matsuoka, S., Nagel, G. A. & Collins, A. Steady-state and dynamic properties of cardiac sodium-calcium exchange. Sodium-dependent inactivation. *J. Gen. Physiol.* **100,** 905–932 (1992).
28. Hilgemann, D. W. & Lu, C. C. Giant membrane patches: improvements and applications. *Methods Enzymol.* **293,** 267–280 (1998).
29. Hilgemann, D. W. Numerical approximations of sodium-calcium exchange. *Prog. Biophys. Mol. Biol.* **51,** 1–45 (1988).

Supplementary Information accompanies the paper on **www.nature.com/nature**.

Acknowledgements We thank S. Feng and P. Foley for technical assistance; K. Philipson for providing the BHK cell line; L. Hrysko for defining NCX1 *I–V*s with organic NCX1 inhibitors; and A. Ferguson and L. DeFelice for critical comments on the manuscript. This work was supported by an NIH grant to D.W.H. and a Samsung Biomedical Research Institute grant to T.M.K.

Competing interests statement The authors declare that they have no competing financial interests.

Correspondence and requests for materials should be addressed to D.W.H. (donald.hilgemann@utsouthwestern.edu).

A proton pore in a potassium channel voltage sensor reveals a focused electric field

Dorine M. Starace & Francisco Bezanilla

Department of Physiology and Department of Anesthesiology, David Geffen School of Medicine at UCLA, Los Angeles, California 90095, USA

Voltage-dependent potassium channels are essential for the generation of nerve impulses[1]. Voltage sensitivity is conferred by charged residues located mainly in the fourth transmembrane segment (S4) of each of the four identical subunits that make up the channel. These charged segments relocate when the potential difference across the membrane changes[2,3], controlling the ability of the pore to conduct ions. In the crystal structure of the *Aeropyrum pernix* potassium channel KvAP[4], the S4 and part of the third (S3B) transmembrane α-helices are connected by a hairpin turn in an arrangement termed the 'voltage-sensor paddle'. This structure was proposed to move through the lipid bilayer during channel activation, transporting positive charges across a large fraction of the membrane[5]. Here we show that replacing the first S4 arginine by histidine in the *Shaker* potassium channel creates a proton pore when the cell is hyperpolarized. Formation of this pore does not support the paddle model, as protons would not have access to a lipid-buried histidine. We conclude that, at hyperpolarized potentials, water and protons from the internal and external solutions must be separated by a narrow barrier in the channel protein that focuses the electric field to a small voltage-sensitive region.

The recently solved complete crystal structure of KvAP[4] did not clarify how the voltage sensor of an ion channel moves charge across the membrane, because the structure was incompatible with the authors' functional data[5]. To reconcile the structural and functional data for KvAP, the authors combined parts of two KvAP structures that were crystallized in different conditions, and used these data to produce their paddle model of activation[5]. This model raises important questions: whether the charged voltage-sensing residues reside in the bilayer, and how far they move when changing from the resting to the active position. These questions can be answered by titrating the voltage-sensing residues with protons by varying the pH of the external and internal medium and then measuring the resulting movement of gating charge. The pK_a values of the naturally occurring arginines are too basic for such a study, so we replaced these residues individually with histidine. Upon histidine replacement of all S4 charges except for the most extracellular one (R362), the S4 acts as a proton transporter[6,7]. Here we extend our study to R362. We find that a histidine at this position also senses voltage and displaces protons, but in a very different way: rather than transporting protons, it forms a proton pore.

Histidine replacement of the first S4 charge, R362, was made in a non-conducting (W434F)[8], non-inactivating (IR, Δ6–46)[9] *Shaker* potassium channel. Figure 1 shows pulse-evoked currents from the R362H mutant recorded using the macropatch technique. In an inward proton gradient, there is a large inward proton current, I_H, whose amplitude at each test pulse is independent of the membrane holding potential (compare Fig. 1a with Fig. 1b). At a holding potential of −90 mV, a steady inward current of 290 pA was recorded (Fig. 1a). Upon return to −90 mV, only pulses greater than −10 mV gave rise to tail currents with opening kinetics, indicating that a channel was fully open at potentials less than −10 mV. In contrast, when the holding potential was 0 mV, there was no steady current and the pulse-elicited currents were activated more quickly as the pulse became negative (Fig. 1b). The voltage dependence of the current, which was measured 40 ms after pulse onset, shows that at negative potentials the currents are essentially ohmic (Fig. 1c), behaviour that is typical of channel conduction.

The conductance of the R362H channel, $G(V)$, is equal to $I_H(V - E_H)$, where V is test pulse potential and E_H is the H^+ equilibrium potential. Conductance increases sharply at approximately −10 mV, and is most voltage dependent between −100 and −10 mV (Fig. 1d). The voltage dependence of conductance is much like a mirror image of the voltage dependence of gating-charge movement, Q, of the *Shaker* potassium channel (Q–V curve; see Fig. 5a). This suggests that the proton current is coupled to voltage-sensor movement. Moreover, the negative shift of −34 mV along the voltage axis in the G–V curve obtained from a holding potential of 0 mV relative to −90 mV (Fig. 1d) corresponds to the same holding-

potential-dependent shift characteristic of the Q–V curve[10]. Finally, the time course of R362H proton channel opening (Fig. 1b) is similar to the time course of the gating-charge movement recorded from the non-conducting *Shaker* channel when held at 0 mV (ref. 10).

The inward rectification of the R362H channel is not due to the H^+ equilibrium potential because even in the presence of an outward proton gradient, the voltage dependence of the proton currents shows inward rectification (Fig. 2a, circles and triangles). Proton gradients were imposed by varying the external pH (pH_o) and keeping the internal solution constant. Because control of internal pH (pH_i) is not precise in the cut-open oocyte voltage-clamp configuration, pH_i was measured with a proton-selective microelectrode. Figure 2b shows three series of R362H tail currents recorded in different proton gradients. When the R362H channel is open at the end of the hyperpolarizing pulse to −120 mV and the membrane potential is suddenly changed, the elicited, instantaneous tail currents, I_{Inst}, are generated by the flow of ions through the open channel down their electrochemical gradients, along with a gating-current component. The gating component was removed from the tail currents by subtracting currents recorded in the presence of 5 mM $NiSO_4$, which blocks proton current through the R362H channel (see below). The voltage dependence of the instantaneous tail currents shows that, for each of the three proton gradients, the tail currents reverse direction (E_{rev}) around the Nernst H^+ equilibrium potential (Fig. 2b). Therefore, the ionic current through the open R362H channel is driven by the H^+ electrochemical gradient, indicating that the R362H current is carried by protons. The protons flow down their electrochemical gradient when the pore is open, so rectification must be imposed by a voltage-dependent mechanism that closes the pore at positive potentials. The most obvious candidate is the introduced histidine: it is charged and because it replaces one of the voltage-sensing residues, it is expected to move in a voltage-dependent way. If so, then hyperpolarized potentials must drive the histidine to a position that creates a proton pore either by bridging the internal and external solutions or by connecting a proton wire. Conversely, depolarized potentials move the histidine away from this narrow transmembrane span or wire and thereby abolish or close the proton pore.

The R362H channel currents can be blocked by the histidine-binding metal nickel, indicating that the proton currents are specific to histidine. Figure 2c shows the voltage-dependent behaviour of the proton currents in pH_o 9.2, 7.4 and 5 before the addition of Ni^{2+} (filled symbols). Addition of 5 mM $NiSO_4$ to the external solution at pH_o 7.4 produced a significant reduction of the proton current (open triangles) indicating direct exposure of the histidine residue to the external solvent. The nickel block could not be removed by washing with an external solution of pH_o 7.4. The block was relieved only by washing with an external solution of pH_o 5 (open squares), indicating that an excess of protons was necessary to compete for the nickel-binding site.

To further verify the involvement of histidine in the R362H proton currents, we examined the channel pK_a by measuring current amplitude as a function of external pH. As shown in Fig. 2d, the modulation of the proton currents by pH_o at a given membrane potential (−130 mV) fitted a two-state model (Henderson–Hasselbach equation) with a pK_a of 6.5, which is consistent with the titration of a histidine residue that is considerably exposed to the external solvent.

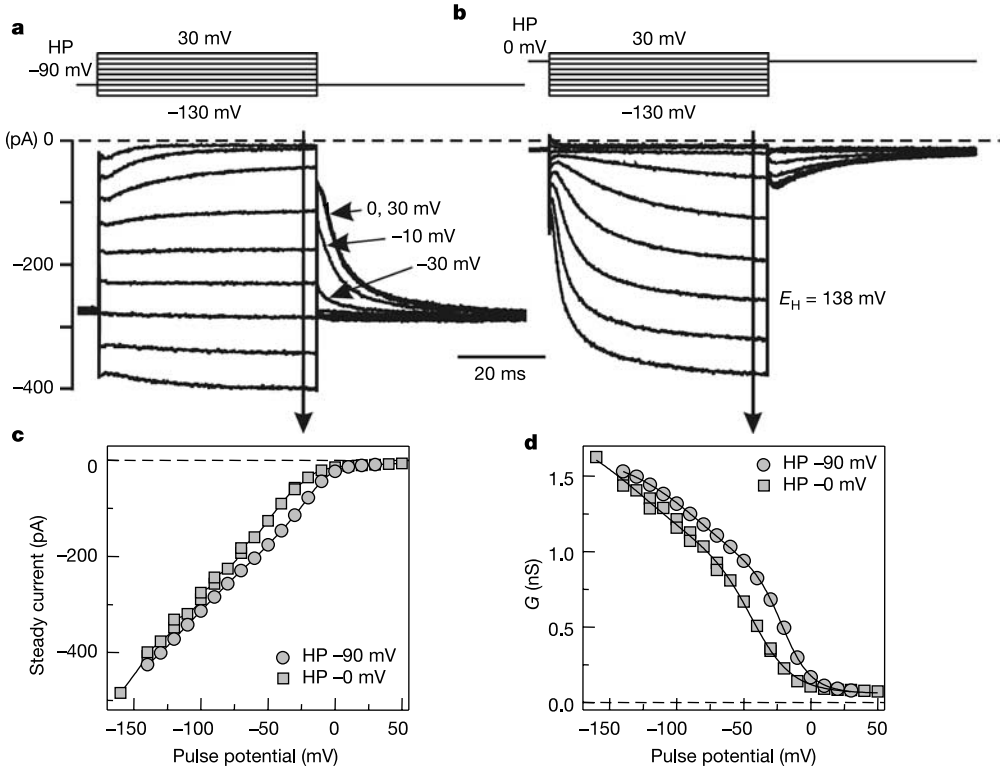

Figure 1 Voltage dependence of proton currents from the R362H *Shaker* channel. Proton currents were measured from a cell-attached macropatch on a perforated oocyte in pH_o 5/pH_i 7.4 solutions. The superimposed currents were elicited by various test pulses, V_t, from a holding potential (HP) of **a**, −90 mV or **b**, 0 mV. **c**, **d**, Voltage dependence of the steady-state proton current amplitudes (indicated by arrows in **a** and **b**) (I–V curves, **c**) and the proton conductance $G(V_t) = I(V_t)/(V_t - E_H)$ (G–V curves, **d**) recorded with a holding potential of −90 mV (circles) and 0 mV (squares). G–V curves were fitted to a sum of two Boltzmann functions (lines).

The voltage at which the proton current turns on increases with decreasing external pH (Fig. 2a, c), another behaviour suggesting that R362H pore formation is coupled to voltage-sensor movement. At pH_o of 7.4, the R362H proton current turns on at approximately −80 mV, a potential at which most of the gating charge is in the closed position, whereas at pH_o 5.1, the currents turn on at approximately −30 mV. This displacement of about 20 mV per pH unit is consistent with the behaviour of voltage-sensor movement, which also shifts positively along the voltage axis with decreasing pH_o owing to surface-charge screening by external protons (by about 13 mV per pH_o unit for another mutant)[7].

The R362H channel proton currents are large, making it imperative that we prove that there is no component of the current going through the K^+ pore of the channel. We therefore examined a 'K-conducting' version of the R362H channel containing a functional K^+ pore with the mutation T449Y (rather than W434F), which increases the affinity of the K^+ pore for the blocker agitoxin II[11]. Figure 3a shows a superimposed set of K^+ currents through the 'K-conducting' R362H channel elicited by the corresponding superimposed test-pulse protocol shown to the right of Fig. 3b, all recorded in solutions containing 120 mM K^+ inside and 2 mM K^+ outside. These currents are robust outward K^+ currents whose voltage dependence and activation kinetics are similar to those of the wild-type *Shaker* potassium channel (with fast inactivation removed). When the channel blocker agitoxin II was added to the external solution, the K^+ pore of the 'conducting' R362H channel was totally blocked (Fig. 3b). The remaining current could still be modulated by the external pH (Fig. 3c) with a pK_a of 6.2 (Fig. 3e), which is indicative of a proton current via the 362H-binding site. Moreover, in all pH gradients (Fig. 3d), the voltage dependence of this remaining current showed the inward rectification observed in the R362H channel containing the K^+-conduction-abolishing mutation W434F. Comparison of the proton current properties in the agitoxin-II-blocked K-conducting channels and the non-conducting R362H channels indicates that the R362H proton pore is distinct from the K^+ pore.

The behaviour of noise fluctuations in the current at steady state was examined because it reflects the underlying microscopic process and can help to distinguish between mechanisms of pore conductance and transport[12,13]. The top of Fig. 4a shows an ensemble of 149 superimposed R362H currents in response to a −130 mV pulse from a holding potential of 0 mV. The power spectrum of the R362H proton channel, calculated from the Fourier transform of the fluctuations of the stationary current, is plotted in Fig. 4a. Simple mechanisms of conduction through a pore give rise to power spectra with lorentzian shapes[12,13], whereas simple mechanisms of transport generate power spectra that rise and plateau with increasing frequency, f (refs 12, 13). The R362H power spectrum fits the expected lorentzian decay of conduction through a pore[13] with a small $1/f$ component[14] (Fig. 4a, line). The rate constant of the rising phase of the proton current is 3.6 ms, which is expected to yield a lorentzian corner frequency of 44 Hz. This is very close to the corner frequency of the fitted lorentzian decay, 33 Hz (Fig. 4a, top), indicating that the opening of the proton conductance is the main gating process at the tested potential.

To estimate the conductance of a single proton channel, we performed non-stationary ensemble mean-variance analysis of R362H channel currents[15]. The top of Fig. 4b shows the mean and variance from a set of 142 R362H currents elicited by repetitive

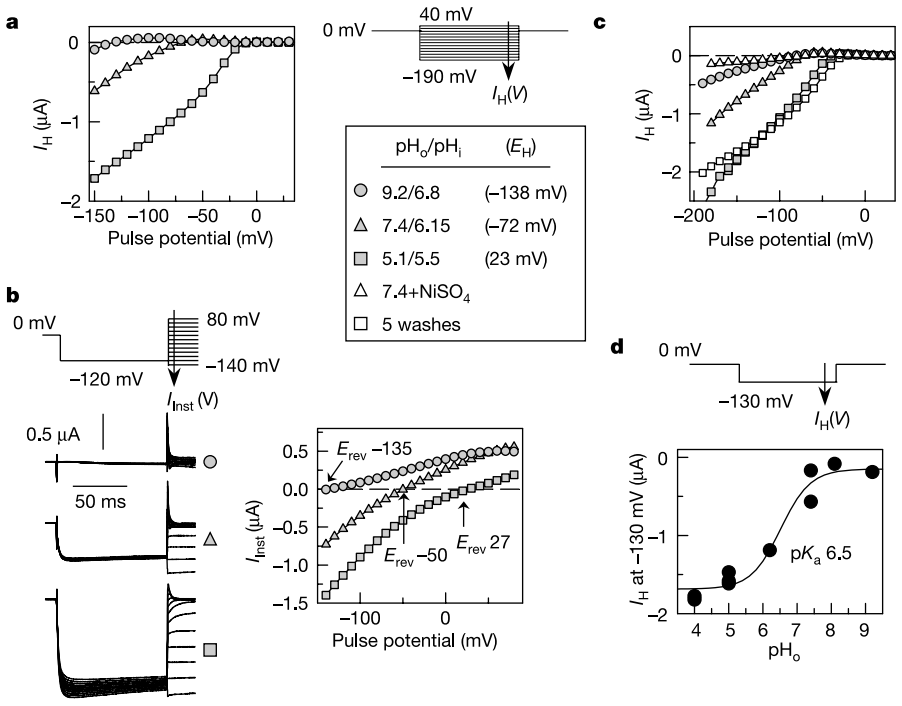

Figure 2 The R362H *Shaker* channel currents are carried by protons and are specific to histidine. *I–V* curves of **a**, steady-state proton currents, I_H, and **b**, instantaneous tail currents, I_{Inst}, recorded in various pH gradients (indicated in box). I_{Inst}–*V* curves (**b**, right) were obtained after subtracting currents (left) recorded in the presence of nickel to eliminate gating currents. Cut-open oocyte voltage-clamp currents were recorded from the same membrane area using the associated pulse protocol shown. The arrow in each pulse protocol represents the isochronal point used to plot current amplitudes for each *I–V* curve. **c**, *I–V* curves of steady-state proton currents recorded, as described in **a**, before, during and after $NiSO_4$ addition. **d**, Proton currents recorded in response to a −130 mV pulse in various values of pH_o. The I_H–pH_o curve was fitted to the Henderson–Hasselbach equation with a pK_a of 6.5: $I = I_{min} + (I_{max} - I_{min})/[1 + \exp(2.3(pH_o - pK_o))]$.

−100 mV test pulses from 0 mV. Fitting the mean-variance curve shown in Fig. 4b revealed that the single-proton-channel current, *i*, at −100 mV was 9 fA, which yields a single-channel conductance of 40 fS (47 ± 13 fS for $n = 5$ experiments). Therefore, at −100 mV, there is a flow of protons at the rate of $i/(ze_0) \approx 56{,}000\ s^{-1}$ (where *z* is the proton valence and e_0 is the electronic charge), which is markedly larger than the value expected of a current arising from transport. In the likely case that the probability of the channel being open at −100 mV is less than 1, the flow rate would be even higher. Both the shape of the R362H channel power spectrum (Fig. 4a) and the conductance of a single proton channel are more consistent with a proton current arising from conduction through a pore rather than from transport. Moreover, the single-channel conductance of each of the four R362H proton channels in the *Shaker* tetramer is about one-quarter that of the proton channel found in eosinophils[16], and is the same as the proton conductance of the gramicidin channel[17].

The properties of the histidine-mediated current of R362H presented here are different from those of the voltage-sensor-coupled proton transport that arises from histidine replacement of the other *Shaker* potassium channel voltage-sensing residues, R365, R368 or R371 (refs 6, 7). An example of the voltage dependence of the proton transport current from the R365H channel is shown in Fig. 5b. The bell shape of the I_H–V curve indicates proton transport. Transport current is maximal in the voltage region where gating-charge movement, *Q*, is steeply voltage dependent (Fig. 5a). In this region, the histidine, coupled to the voltage sensor, makes frequent transitions between open and closed states and can transport protons, one at a time, across the membrane, with each transition in the direction of the H^+ electrochemical gradient. The transport current drops to zero at very hyperpolarized and depolarized potentials, where the histidine, coupled to the voltage sensor, favours one state and transitions to other states become minimal. By contrast, the voltage dependence of the R362H proton currents is not bell-shaped and does not saturate at hyperpolarized potentials (Fig. 5c), a behaviour like that of an inwardly rectifying channel. We have provided evidence that the R362H currents arise from conduction through a voltage-gated pore rather than from transport with each voltage-sensor stroke. Even if conduction involves a proton-shuttle mechanism in which the histidine side chain rotates at equilibrium to alternative positions, such a conduction mechanism is distinct from voltage-driven transport.

Conduction or transport of protons by the histidine-tagged voltage sensor has important implications for its conformational changes. For proton transport to occur (Fig. 5b), the histidine must move from internal to external access with each voltage-sensor transition. Such access may occur through proton wire networks in the protein or through aqueous crevices that penetrate the hydrophobic environment and reach the voltage-sensing residues. The latter possibility is supported by other experimental evidence[6,7,18,19]. Figure 5d shows a model of voltage-sensor movement in which the histidine-replaced residues can transport protons; depolarization of the membrane moves the histidine (filled circle), along with the other voltage-sensing residues (open circles), from an internally facing aqueous crevice to an externally facing cavity. The transfer of

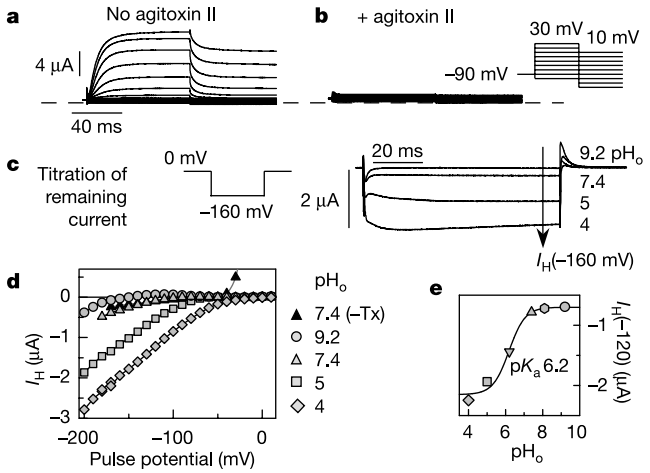

Figure 3 The R362H proton channel is distinct from the potassium channel. Cut-open voltage clamp K^+ currents recorded from the 'K-conducting' version of the R362H channel before (**a**) and after (**b**) external agitoxin II addition to a concentration of 1 μM. The pulse protocol is shown on the right. Currents were recorded in pH_o 7.4, 120 mM K^+ inside and 2 mM K^+ outside. **c**, pH_o titratable currents elicited by hyperpolarizing test pulses from 0 mV remained after agitoxin block of the K^+ pore. **d**, *I*–*V* curves of steady-state proton currents, I_H, recorded in different pH gradients generated from pulse-elicited currents from 0 mV after agitoxin block. (Agitoxin was absent in the '−Tx' curve, from −90 mV.) **e**, After the agitoxin block, pH_o modulation of proton currents elicited by −120 mV pulses fitted the Henderson–Hasselbach equation with a pK_a of 6.2.

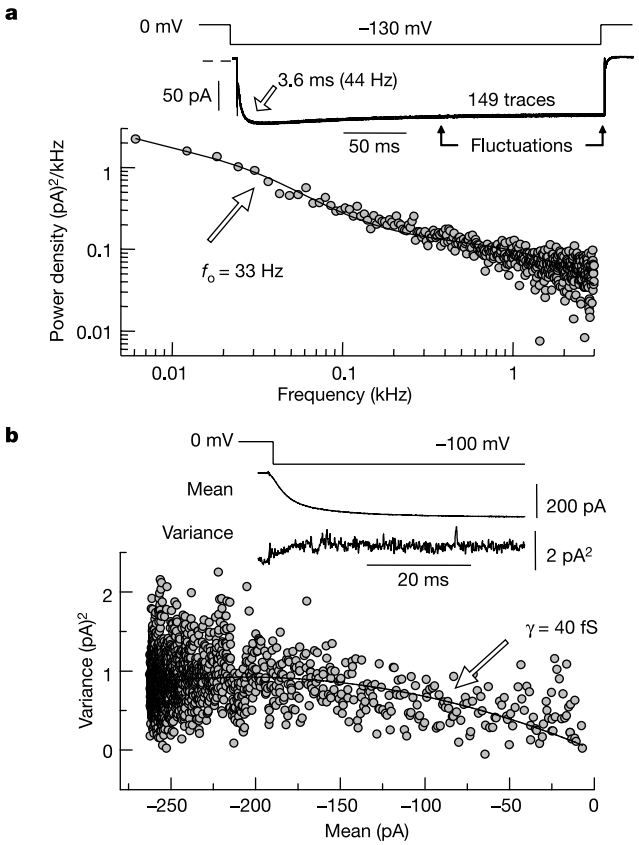

Figure 4 Biophysical properties reveal the nature of the R362H proton current. **a**, Top, an ensemble of 149 R362H currents recorded in pH_o 5/pH_i 9.2, elicited by repetitive pulses to −130 mV from a holding potential of 0 mV. Bottom, power spectrum of the stationary current fluctuations. **b**, Top, time course of the mean and variance from a set of 142 R362H currents, recorded in pH_o 5/pH_i 7.4 and elicited by repetitive −100 mV pulses from 0 mV. Bottom, plot of the mean versus variance at each time point, and the best fit to a parabolic function (line) predicts a single-proton-channel current of $i = 9$ fA and $N = 46{,}000$ proton channels.

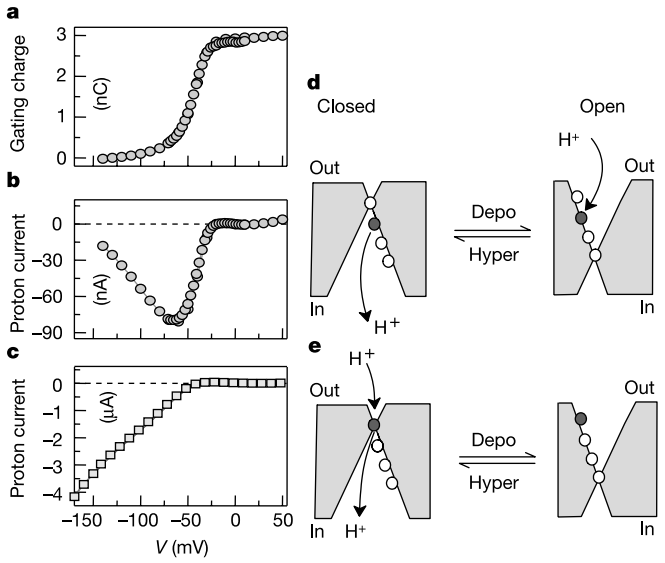

Figure 5 Proton transport and conduction: models of the conformational changes of the voltage sensor. **a**, Voltage dependence of the gating-charge movement of the *Shaker* R365H channel. **b**, Voltage dependence of proton-transport current of the R365H channel. **c**, Voltage dependence of proton channel current of the R362H channel. **d**, Conformational changes during proton transport. In a proton gradient (inward), the histidine at 365 (filled circle) transports one proton each time the voltage sensor goes from the open to the closed conformation. **e**, Representation of the R362H channel proton pore. Internal and external protons have simultaneous access to the histidine (filled circle) only in the closed position, which results in a continuous proton current when the sensor is closed. The protein core is grey. 'Depo' and 'hyper' indicate a more positive and a more negative membrane potential, respectively.

charge across the membrane in this model may be achieved by a relatively small conformational change[20,21].

Proton conduction by R362H imposes a particularly stringent constraint on voltage-gating models because, in the open proton pore, site 362 has to be simultaneously accessible from both sides of the membrane. This constraint is shown in Fig. 5e: when the R362H proton channel is open at hyperpolarized potentials, the histidine bridges the two water-filled crevices, thus creating a proton-selective pore. Depolarization closes the proton channel by moving 362H away from the pore-permissive bridge. The narrow membrane span necessary to create a proton pore at 362H implies that the transmembrane electric field is concentrated near the histidine. Such increased field strength has been measured directly with site-directed voltage-sensitive probes[19]. The focused field makes the structure exquisitely voltage sensitive and places constraints on the conformational rearrangements that the voltage sensor undergoes. A small conformational change can move the large amount of necessary gating charge across the focused transmembrane field. When histidine replaced the fourth S4 charge (R371H), both proton transport and conduction were observed[6]. However, proton conduction was small and occurred only at very depolarized potentials, a result that has also been incorporated into our model (Fig. 5d, e).

The results and implications of the R362H proton pore can be put in the context of the recently obtained crystal structures of the KvAP channel[4]. In the paddle model of channel activation, the charged residues of S4 are not exposed to the intracellular solution at all because the authors found that the S3B–S4 loop is not internally accessible to site-specific Fab fragments[5], nor are there potential proton wire pathways in the closed state. The paddle model would require drastic modifications to accommodate movement of residues at positions 365, 368 and 371 across the bilayer from internal to external proton access[6,7]. One modification could be a deformation of the bilayer to allow a closer approach of the charged residues to protons that may penetrate with water at the edges of the membrane. However, even a modified paddle model could not be reconciled with the ability of the R362H channel to form a proton pore, because the integrity of the protein/bilayer in the paddle model is not broken by aqueous crevices to allow the required proton access to 362H from both sides of the membrane at negative potentials (Fig. 5e). It is important to note that the paddle model is based on docking the crystal structure of the isolated KvAP S1–S4 fragment to the pore region of the entire KvAP crystal in a particular conformation that is not unique[5]. As many other conformations are clearly possible, molecular modelling constrained by functional and structural data will most probably predict other structures that will expand the picture of possible voltage-sensor movements during activation, so that a model consistent with the constraints imposed by the R362H proton pore will emerge. One such structure, which is qualitatively compatible with our results, proposes that S4 adopts a transmembrane orientation and is packed against the pore domain near the interface between adjacent subunits[22].

The results presented here on the behaviour of a proton pore created artificially from the voltage sensor of a potassium channel may have implications beyond the structure of the voltage sensor. Operation of this proton pore has revealed a unique and fundamental structural feature that may be very useful in understanding the structure–function relationship of naturally occurring voltage-dependent proton channels[23]. □

Methods

Mutagenesis and expression of channels

Unless otherwise mentioned, the clone that was used as the background template for R362H mutagenesis contained the non-conducting (W434F)[8], non-inactivating (IR, Δ6–46)[9] *Shaker* H4 potassium channel coding sequence[7,24]. The 'K-conducting' version of the R362H channel contained the pore mutation T449Y, but not W434F. The R362H mutation was generated by overlap extension polymerase chain reaction (PCR)[25] followed by mutagenic fragment replacement. All sequences generated by PCR were sequenced. To express the channel, complementary RNA was transcribed from the *Not*I-linearized DNA clone (New England Biolabs) with T7 RNA polymerase (Message Machine *in vitro* transcription kit from Ambion) and 50 nl of 0.5–0.8 $\mu g\,\mu l^{-1}$ cRNA was injected into each stage-5 *Xenopus* oocyte[26]. Injected oocytes were maintained at 18 °C in an incubation solution of 100 mM NaCl, 2 mM KCl, 1.8 mM $CaCl_2$, 1 mM $MgCl_2$, 5 mM HEPES (pH 7.3), 0.010 mM EDTA and 0.5 mM DTT. The incubation solution was changed daily.

Electrophysiology

Channel currents were measured from oocytes 3 to 6 days after the injection of channel cRNA. Currents were recorded at 20–23 °C with the cut-open oocyte voltage-clamp technique[6,27] or with the patch-clamp technique[6,28]. Data were filtered at one-fifth the sampling frequency. Currents were recorded unsubtracted after analogue compensation of linear membrane capacitance at 0–50 mV. There was no subtraction or compensation of linear leak components while recording; these were subtracted off-line[6]. Unless otherwise stated, the external solutions contained 120 mM *n*-methylglucamine (NMDG), 2 mM $CaCl_2$, and either 20 mM CHES (2-(*N*-cyclohexylamino)ethanesulphonic acid, pH 9.2) or 20 mM HEPES (all other pHs); all solutions were brought to the appropriate pH with methanesulphonic acid (Fluka). The internal solutions were the same as the external solutions except that EGTA–NMDG replaced $CaCl_2$. The osmolarity of all recording solutions was 240–260 mosM. All of the experiments reported here were reversible with respect to the effect of pH. Electrophysiological acquisition and analysis software were home-made.

In cut-open oocyte voltage clamps, the pH_i of the oocyte, monitored with an H^+ electrode impaling the oocyte during current recordings, varies between pH 5.8 and 7.3 regardless of the pH of the internal solution used[6]. Therefore, for the recordings shown in Fig. 2a, b, a second intracellular electrode, filled with a liquid ion-exchanger resin selective for H^+ (IE010 from WPI, Inc.), was used to measure pH_i[6]. The H^+ electrode was mounted on the amplifier (Dagan) on the current electrode headstage for two-electrode clamp.

Stationary (Fig. 4a) and non-stationary noise analysis (Fig. 4b) were carried out using the patch-clamp technique in the cell-attached mode with oocytes that were ruptured to expose the internal contents to the bath solution. From a holding potential of 0 mV, a set of 100–300 proton current traces was recorded by repetitively hyperpolarizing the membrane to −100 to −160 mV every second. For stationary noise-fluctuation analysis, sets of repetitively pulsed currents were recorded in response to hyperpolarizing test pulses of 300 ms duration. Acquired data were filtered at 2.5 kHz. The power spectrum of R362H currents was determined from a fast Fourier transform of the final 150–160 ms of the 300 ms pulse-elicited currents. The power spectrum was fitted to a sum of two lorentzian

functions and a 1/*f* component. For non-stationary noise analysis, sets of repetitively pulsed currents were recorded in response to hyperpolarizing test pulses of 50 ms duration. Acquired data were filtered at 5–10 kHz. Mean current (I) and variance (σ^2) were calculated from successive pairs of current traces to minimize the effect of drift during the time taken to record the entire ensemble of currents. The single-proton-channel current (or the single-subunit current), i, and the number of proton channels (or subunits), N, was determined by fitting the $\sigma^2 - I$ plot to the equation $\sigma^2 = iI - I^2/N + B$, where B is a background-noise term.

Agitoxin II preparation

Synthetic agitoxin II was expressed and purified as a cleavable fusion protein in *Escherichia coli* according to the protocol described in ref. 29. The agitoxin expression clone was generously provided by A. Gross[30].

Received 22 August; accepted 5 December 2003; doi:10.1038/nature02270.

1. Hodgkin, A. L. & Huxley, A. F. A quantitative description of membrane current and its application to conduction and excitation in nerve. *J. Physiol. (Lond.)* **117,** 500–544 (1952).
2. Seoh, S.-A., Sigg, D., Papazian, D. M. & Bezanilla, F. Voltage-sensing residues in the S2 and S4 segments of the *Shaker* K^+ channel. *Neuron* **16,** 1159–1167 (1996).
3. Aggarwal, S. K. & MacKinnon, R. Contribution of the S4 Segment to gating charge in the *Shaker* K^+ channel. *Neuron* **16,** 1169–1177 (1996).
4. Jiang, Y. *et al.* X-ray structure of a voltage-dependent K^+ channel. *Nature* **423,** 33–41 (2003).
5. Jiang, Y., Ruta, V., Chen, J., Lee, A. & MacKinnon, R. The principle of gating charge movement in a voltage-dependent K^+ channel. *Nature* **423,** 42–48 (2003).
6. Starace, D. M. & Bezanilla, F. Histidine scanning mutagenesis of basic residues of the S4 segment of the *Shaker* K^+ channel. *J. Gen. Physiol.* **117,** 469–490 (2001).
7. Starace, D. M., Stefani, E. & Bezanilla, F. Voltage-dependent proton transport by the voltage sensor of the *Shaker* K^+ channel. *Neuron* **19,** 1319–1327 (1997).
8. Perozo, E., MacKinnon, R., Bezanilla, F. & Stefani, E. Gating currents from a non-conducting mutant reveal open–closed conformations in *Shaker* K^+ channels. *Neuron* **11,** 353–358 (1993).
9. Hoshi, T., Zagotta, W. N. & Aldrich, R. W. Biophysical and molecular mechanisms of *Shaker* potassium channel inactivation. *Science* **250,** 533–538 (1990).
10. Olcese, R., Latorre, R., Toro, L., Bezanilla, F. & Stefani, E. Correlation between charge movement and ionic current during slow inactivation in *Shaker* K^+ channels. *J. Gen. Physiol.* **110,** 579–590 (1997).
11. Gross, A. & MacKinnon, R. Agitoxin footprinting the *Shaker* potassium channel pore. *Neuron* **16,** 399–406 (1996).
12. Lee, Y. W. *Statistical Theory of Communication* (Wiley, New York, 1960).
13. Stevens, C. F. Inferences about membrane properties from electrical noise measurements. *Biophys. J.* **12,** 1028–1047 (1972).
14. Conti, F., Neumcke, B., Nonner, W. & Stampfli, R. Conductance fluctuations from the inactivation process of sodium channels in myelinated nerve fibers. *J. Physiol. (Lond.)* **308,** 217–239 (1980).
15. Sigworth, F. J. The variance of sodium current fluctuations at the node of Ranvier. *J. Physiol. (Lond.)* **307,** 97–129 (1980).
16. Cherny, V. V., Murphy, R., Sokolov, V., Levis, R. A. & DeCoursey, T. E. Properties of single voltage-gated proton channels in human eosiniphils estimated by noise analysis and by direct measurement. *J. Gen. Physiol.* **121,** 615–627 (2003).
17. Schumaker, M. F., Pomès, R. & Roux, B. A. Combined molecular dynamics and diffusion model of single proton conduction through gramicidin. *Biophys. J.* **79,** 2840–2857 (2000).
18. Islas, L. D. & Sigworth, F. J. Electrostatics and the gating pore of *Shaker* potassium channels. *J. Gen. Physiol.* **117,** 69–89 (2001).
19. Asamoah, O. K., Wuskell, J. P., Loew, L. M. & Bezanilla, F. A fluorometric approach to local electric field measurements in a voltage-gated ion channel. *Neuron* **37,** 85–97 (2003).
20. Yellen, G. The moving parts of voltage-gated ion channels. *Q. Rev. Biophys.* **31,** 239–295 (1998).
21. Bezanilla, F. The voltage sensor in voltage-dependent ion channels. *Physiol. Rev.* **80,** 555–592 (2000).
22. Laine, M. *et al.* Atomic proximity between S4 segment and pore domain in *Shaker* potassium channels. *Neuron* **39,** 467–481 (2003).
23. DeCoursey, T. E. Voltage-gated proton channels and other proton transfer pathways. *Physiol. Rev.* **83,** 475–579 (2003).
24. Schwarz, T. L., Tempel, B. L., Papazian, D. M., Jan, Y. & Jan, L. Y. Multiple potassium-channel components are produced by alternative splicing at the *Shaker* locus in *Drosophila*. *Nature* **331,** 137–142 (1988).
25. Ho, S. N., Hunt, H. D., Horton, R. M., Pullen, J. K. & Pease, L. R. Site-directed mutagenesis by overlap extension using the polymerase chain reaction. *Gene* **77,** 51–59 (1989).
26. Timpe, L. C. *et al.* Expression of functional potassium channels from *Shaker* cDNA in *Xenopus* oocytes. *Nature* **331,** 143–145 (1988).
27. Stefani, E. & Bezanilla, F. The cut-open oocyte voltage clamp technique. *Methods Enzymol.* **293,** 300–318 (1998).
28. Hamill, O. P., Marty, A., Neher, E., Sackmann, B. & Sigworth, F. J. Improved patch-clamp techniques for high-resolution current recording from cells and cell-free membrane patches. *Pflugers Arch.* **391,** 85–100 (1981).
29. Park, C.-S., Hausdorff, S. F. & Miller, C. Design, synthesis, and functional expression of a gene for charybdotoxin, a peptide blocker of K^+ channels. *Proc. Natl Acad. Sci. USA* **88,** 2046–2050 (1991).
30. Garcia, M. L., Garcia-Calvo, M., Hidalgo, P., Lee, A. & MacKinnon, R. Purification and characterization of three inhibitors of voltage-dependent K^+ channels from *Leiurus quinquestriatus* var. *hebraeus* venom. *Biochemistry* **33,** 6834–6839 (1994).

Acknowledgements This work was supported by the National Institutes of Health.

Competing interests statement The authors declare that they have no competing financial interests.

Correspondence and requests for materials should be addressed to F.B. (Fbezanil@ucla.edu).

Dephosphorylated SRp38 acts as a splicing repressor in response to heat shock

Chanseok Shin*, Ying Feng* & James L. Manley

Department of Biological Sciences, Columbia University, New York, New York 10027, USA

* These authors contributed equally to this work

The cellular response to stresses such as heat shock involves changes in gene expression[1]. It is well known that the splicing of messenger RNA precursors is generally repressed on heat shock[2,3], but the factors responsible have not been identified[4–8]. SRp38 is an SR protein splicing factor[9,10] that functions as a general repressor of splicing. It is activated by dephosphorylation and required for splicing repression in M-phase cells[11]. Here we show that SRp38 is also dephosphorylated on heat shock and that this dephosphorylation correlates with splicing inhibition. Notably, depletion of SRp38 from heat-shocked cell extracts derepresses splicing, and adding back dephosphorylated SRp38 specifically restores inhibition. We further show that dephosphorylated SRp38 interacts with a U1 small nuclear ribonucleoprotein particle (snRNP) protein, and that this interaction interferes with 5′-splice-site recognition by the U1 snRNP. Finally, SRp38-deficient DT40 cells show an altered cell-cycle profile consistent with a mitotic defect; they are also temperature sensitive and defective in recovery after heat shock. SRp38 thus plays a crucial role in cell survival under stress conditions by inhibiting the splicing machinery.

To examine whether the splicing repressor SRp38 functions in the inhibition of splicing that occurs after heat shock, we first examined whether the phosphorylation status of SRp38 changes in response to heat shock. SRp38 was efficiently dephosphorylated (dSRp38) when HeLa cells were incubated at 43 °C for durations of up to 1 h, whereas the phosphorylation status of classical SR proteins changed only modestly (Fig. 1a). The pattern of SRp38 dephosphorylation was distinct from that observed in mitosis[11] because, in addition to the fully dephosphorylated isoform, a partially dephosphorylated form accumulated in heat-shocked cells. Incubation of HeLa cells at higher temperatures (such as 46 °C) resulted in a much faster appearance of dSRp38 (data not shown).

We next tested whether SRp38 dephosphorylation could be induced by heat treatment of HeLa nuclear extract. This would allow us to rule out the possibility that the accumulation of dSRp38 requires new protein synthesis and/or the activity of classical heat-shock proteins, which are excluded from the nucleus before heat shock[12,13]. Standard HeLa nuclear extract was incubated at 46 °C for 5–25 min and used to measure the phosphorylation status of SRp38 and splicing proficiency (at 30 °C). Splicing was rapidly and completely inhibited, and SRp38 was equally rapidly dephosphorylated (Fig. 1b, c).

We also 'heat-shocked' nuclear extract (46 °C for 5 min) and compared splicing and SRp38 phosphorylation over time with untreated extracts. A typical splicing profile was observed in the control extract, whereas almost complete inhibition was observed in the heat-shocked extract (Fig. 1d). Notably, SRp38 seemed to be fully phosphorylated in the control extract throughout the incubation, but was considerably dephosphorylated in the heat-shocked extract; in fact, dephosphorylation increased slightly during the time course (Fig. 1e). The phosphorylation status of another SR protein, ASF/SF2, did not change detectably in either extract. We also examined splicing and SRp38 phosphorylation status in